

# Finite element analysis of slender HSS columns strengthened with high modulus composites

Amr Shaat<sup>†</sup> and Amir Fam<sup>‡</sup>

Department of Civil Engineering, Queen's University, Kingston, ON, Canada K7L 3N6

(Received July 21, 2005, Accepted September 28, 2006)

**Abstract.** This paper presents results of a non-linear finite element analysis of axially loaded slender hollow structural section (HSS) columns, strengthened using high modulus carbon-fiber reinforced polymer (CFRP) longitudinal sheets. The model was developed and verified against both experimental and other analytical models. Both geometric and material nonlinearities, which are attributed to the column's initial imperfection and plasticity of steel, respectively, are accounted for. Residual stresses have also been modeled. The axial strength in the experimental study was found to be highly dependent on the column's imperfection. Consequently, no specific correlation was established experimentally between strength gain and amount of CFRP. The model predicted the ultimate loads and failure modes quite reasonably and was used to isolate the effects of CFRP strengthening from the columns' imperfections. It was then used in a parametric study to examine columns of different slenderness ratios, imperfections, number of CFRP layers, and level of residual stresses. The study demonstrated the effectiveness of high modulus CFRP in increasing stiffness and strength of slender columns. While the columns' imperfections affect their actual strengths before and after strengthening, the percentage gain in strength is highly dependent on slenderness ratio and CFRP reinforcement ratio, rather than the value of imperfection.

**Keywords:** finite element; retrofit; HSS; slender; column; CFRP; imperfection; residual stresses.

---

## 1. Introduction

Steel columns of medium to high slenderness ratios are commonly used in steel structures and are generally governed by overall buckling failure before developing their full plastic capacity. Conventional strengthening techniques for steel structures, in general, involve bolting or welding additional steel plates. These techniques have a number of shortcomings, including the added self weight of steel plates, installation time, difficulty of shaping and fitting complex profiles, and the need for elaborate and expensive shoring systems. The use of fiber-reinforced polymer (FRP) sheets or strips of adequate stiffness could be quite suitable in such applications, particularly due to their excellent corrosion resistance and superior fatigue properties (Shaat *et al.* 2004).

An experimental study was performed by Shaat and Fam (2006) to investigate the effect of adhesively bonded high modulus carbon-FRP (CFRP) longitudinal sheets on the behavior of axially loaded slender hollow structural section (HSS) columns. The column's cross sectional shape is shown in Fig. 1(a) and the

---

<sup>†</sup>Doctoral Candidate, E-mail [amr@civil.queensu.ca](mailto:amr@civil.queensu.ca)

<sup>‡</sup>Associate Professor, Corresponding Author, E-mail: [fam@civil.queensu.ca](mailto:fam@civil.queensu.ca)

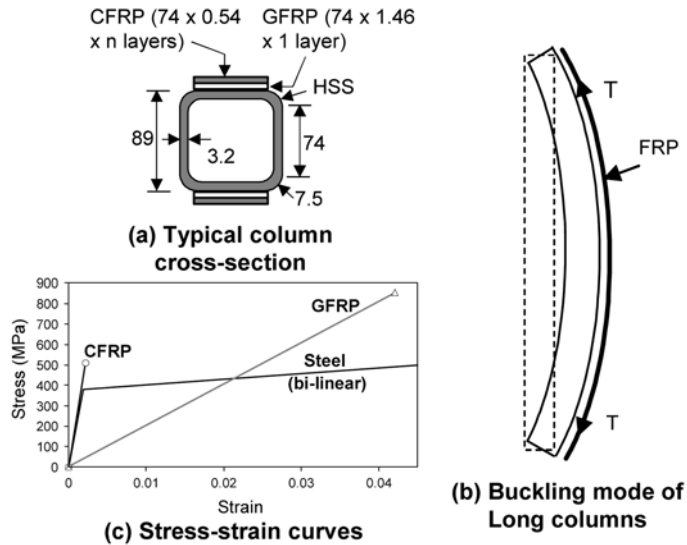


Fig. 1 Test specimens, buckling mode and material properties

column length was 2380 mm, resulting in slenderness ratio of 68. In slender columns, where overall buckling governs, it is anticipated that high modulus CFRP sheets would contribute to the flexural stiffness of the column, and at large lateral displacements for columns with high slenderness ratios could resist some tension on the outer surface, as shown schematically in Fig. 1(b). It was shown in this experimental study that CFRP sheets have indeed increased the columns' strengths by up to 23 percent. However, the study revealed the sensitivity of axially loaded slender columns to their inherent geometric out-of-straightness and alignment (imperfections), which affect both the ultimate strength and lateral displacement of the specimens. Residual stresses are also an important factor, which can affect the behavior of cold-formed columns. While the major parameter intended in the experimental investigation was the effect of number of CFRP layers, it is believed that the geometric imperfections have also varied inevitably among the specimens. Therefore, no specific correlation could be established between the amount of strength gain and the amount of CFRP. As such, it was decided to use a numerical approach, namely the finite element analysis (FEA) to model the specimens and isolate the effect of geometric imperfections from the effect of number of CFRP layers, in order to provide an accurate assessment of the strengthening effectiveness using CFRP. The FEA approach was employed by several other researchers to model steel structures retrofitted by FRP materials, mainly for steel girders, and showed excellent results (Sen *et al.* 2001, Abushaggur and Eldamatty 2003, and Jun Deng *et al.* 2004). The finite element model (FEM) used in this study was first verified against both the column test results and the predictions using another analytical model developed by the authors (Shaat and Fam 2007). As the experimental program was limited to a small number of specimens, the FEM was used to conduct a parametric study to investigate the effects of the number of CFRP layers, value of initial geometric imperfections, level of residual stresses and the columns' slenderness ratios.

This paper first summarizes the experimental research program, and then a discussion of various aspects of the finite element modeling is presented. This is followed by the results of the FEA in terms of load-displacement curves as well as deformed shapes and failure modes. Finally the parametric study and conclusions are presented.

## 2. Summary of experimental investigation

A brief summary of the experimental study is presented in this section, whereas more details can be found elsewhere (Shaath and Fam 2006). The experimental study included 5 slender column tests, conducted on a standard  $89 \times 89 \times 3.2$  mm HSS section (Fig. 1(a)), with yield strength,  $F_y$ , of 380 MPa. The length of the pin-ended columns was 2380 mm, which corresponds to a slenderness ratio of 68. High modulus unidirectional carbon fibre sheets were bonded to the specimens in the longitudinal direction. A single composite layer was 0.54 mm thick and had tensile strength and modulus of 510 MPa and 230 GPa, respectively. A layer of glass-FRP (GFRP) sheet was first installed directly on the steel surface before applying the CFRP layers to prevent direct contact between carbon fibres and steel, which could lead to galvanic corrosion. The GFRP lamina was 1.46 mm thick and had tensile strength and modulus of 855 MPa and 20.3 GPa, respectively. The stress-strain curves of steel (idealized), CFRP, and GFRP are illustrated in Fig. 1(c).

The tested columns included a control (unstrengthened) specimen and three specimens strengthened with one, three and five layers of CFRP, applied on two opposite sides in the plane of overall buckling. The fifth specimen was strengthened with three layers, applied on all four sides of the column. The specimens were given identification codes. For example, 3L-2S indicates three CFRP layers applied on two opposite sides of the column.

The experimental curves of load versus both axial and lateral displacements at mid-length of all specimens are shown in Figs. 2 and 3, along with the numerical and analytical curves, which will be discussed later. The gain in axial strength of the CFRP-strengthened specimens ranged from 13 to 23 percent, as shown in Table 1. The strength gains, however, did not correlate directly to the number of CFRP layers. As indicated earlier, this was attributed to the variability of geometric imperfections among the specimens, which is usually due to a slight out of straightness of different values (Kulak and Grondin 2002), or minor inevitable misalignment within the test setup, or a combination of both. In all specimens,

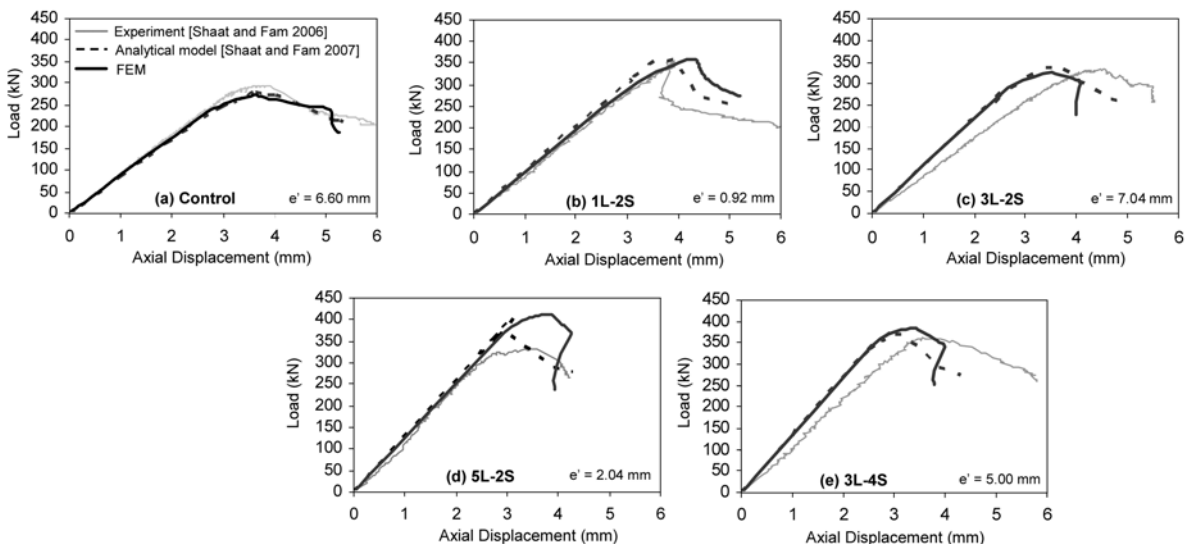


Fig. 2 Load-axial displacement responses

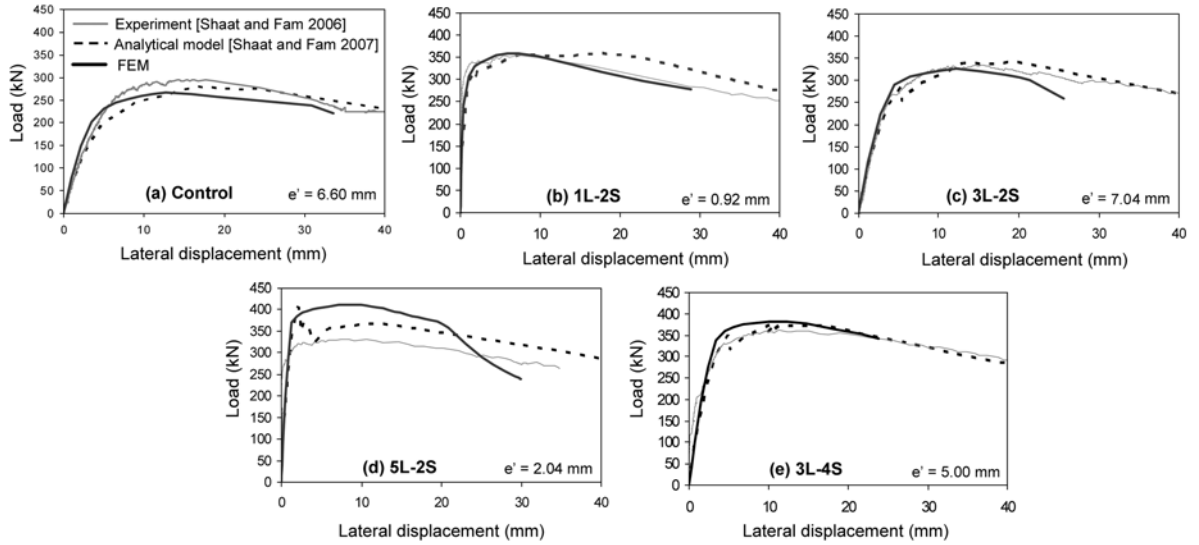


Fig. 3 Load-lateral displacement responses

Table 1 Summary of experimental results

Specimen I.D.	Maximum Load $P_{max}$ (kN)	% age Gain in Strength	Lateral displacement (e) at $P_{max}$ (mm)
Control	295	---	14.22
1L-2S	355	20	7.17
3L-2S	335	14	14.57
5L-2S	332	13	10.66
3L-4S	362	23	11.26

failure was mainly due to excessive overall buckling, as shown in Fig. 4(a), followed by a secondary local buckling in the compression side, at or near mid-length of the specimen. The local buckling took the form of inward buckling of the compression face and outward buckling of the two side faces, which was clearly revealed after testing by cutting the specimen, as shown in Fig. 4(b). For the FRP-strengthened specimens, the secondary local buckling in the compression side resulted in a combined delamination and premature crushing of the FRP sheets. By carefully examining the experimental strains, an average strain of 0.13% can be defined as the strain at which CFRP failed in compression. This strain is limited to this particular case, and may vary for different types of CFRP or HSS sections. No signs of FRP failure have been observed on the tension side.

### 3. Finite element model

The non-linear finite element analysis program ANSYS was used to model the behavior, ultimate load, and failure mode of the pin-ended HSS slender steel columns. The numerical simulation consisted of two stages. In the first stage, an eigenvalue elastic buckling analysis was performed on a perfectly straight

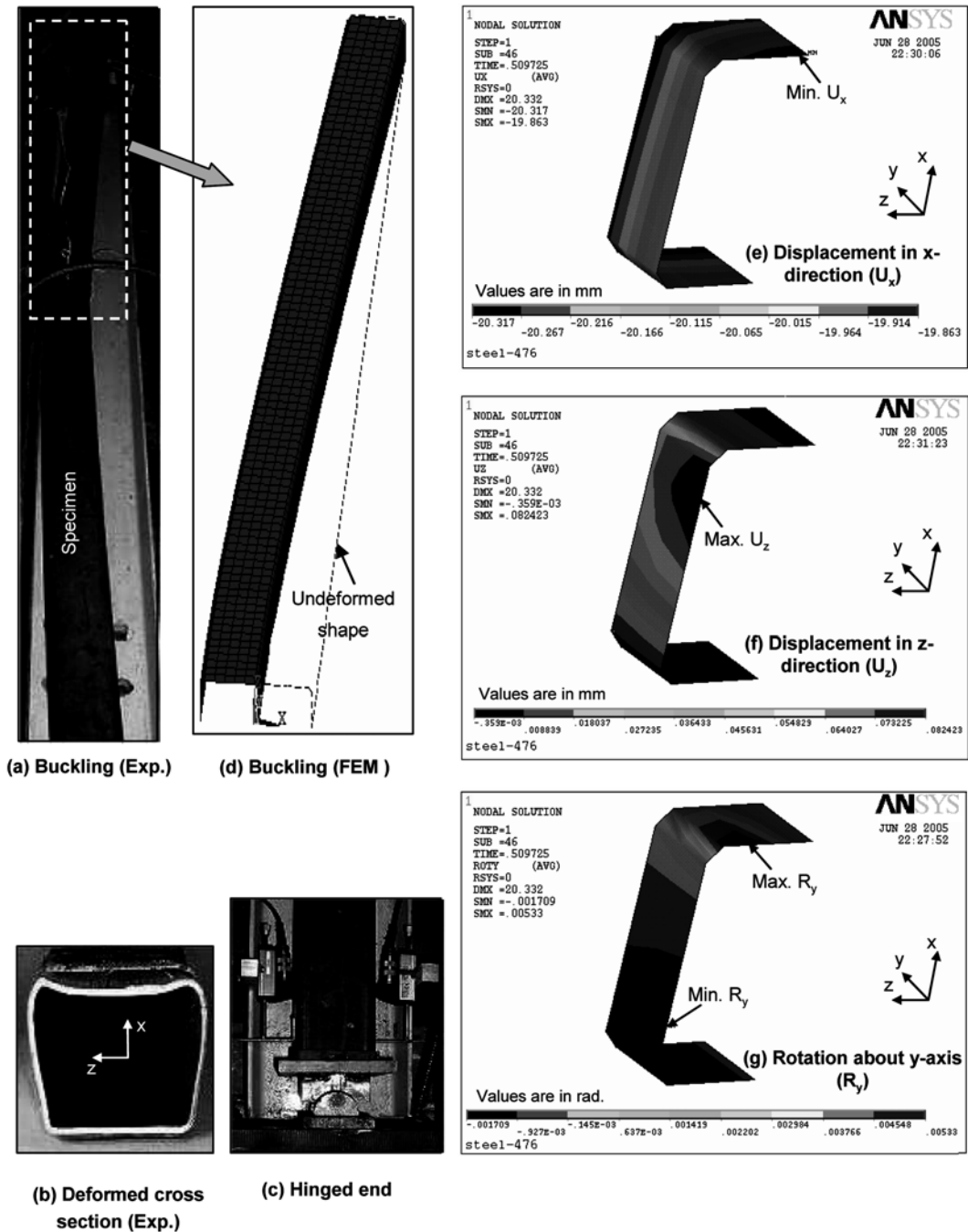


Fig. 4 Comparison between experimental and FEM deformed shapes

specimen, including modeling the entire cross section, to establish the probable buckling modes of the column. The analysis showed that the specimen with slenderness ratio of 68 experienced overall buckling as was also shown experimentally. In the second stage, a non-linear analysis was performed on columns

modeled with geometric imperfections to promote the predicted buckling shape established through the first stage of analysis. In the second stage, the models were loaded to failure to predict the full responses and ultimate loads of the columns, and in this stage, the analysis incorporated both geometric and material non-linearities. The centerline dimensions of the cross-sections and the base metal thickness were used in the geometric modeling, based on the measured cross-sectional dimensions of the specimens. The following sections briefly address various aspects of the finite element modeling, such as element type, mesh density, boundary conditions, material properties, geometric imperfections, and residual stresses.

### 3.1 Elements types and mesh density

An eight-node quadrilateral layered shell element (SHELL91) was used for the steel section in this model. The element configurations as well as its coordinate system are shown in Fig. 5(a). Each node has six degrees of freedom, namely three translations ( $U_x$ ,  $U_y$ , and  $U_z$ ) and three rotations ( $R_x$ ,  $R_y$ , and  $R_z$ ). The multiple layers of the element were utilized to account for residual stress distribution through the steel wall thickness, as will be discussed later. The FRP reinforcing material was modeled using three-dimensional two-node uniaxial truss element (LINK8), as shown in Fig. 5(b). This is considered reasonable because of the small flexural rigidity of the thin CFRP layers. Each node has three degrees of freedom, namely translations in the nodal  $x$ ,  $y$ , and  $z$  directions ( $U_x$ ,  $U_y$ , and  $U_z$ ). Perfect bond between steel and FRP sheets was assumed by defining one node for both SHELL91 and LINK8 elements having the same coordinates. This assumption is quite reasonable as no signs of delamination were observed experimentally, except at the very end when local buckling occurred (i.e., well beyond the peak load).

One quarter of the specimen was modeled, as shown in Fig. 6(a), by taking advantage of the double symmetry of the column. Three preliminary numerical simulations of different mesh densities were first carried out by varying the size of the elements in the HSS flanges and their curved conjunction to the webs, namely mesh #1, mesh #2, and mesh #3, as shown in Fig. 6(b). The number of elements varied from 1050 elements in the first mesh to 4730 elements in the third mesh. The predicted load-lateral displacement behavior using the three numerical simulations for the control HSS column is shown in Fig. 6(c). The figure shows almost identical results, where no change in behavior occurs by refining the

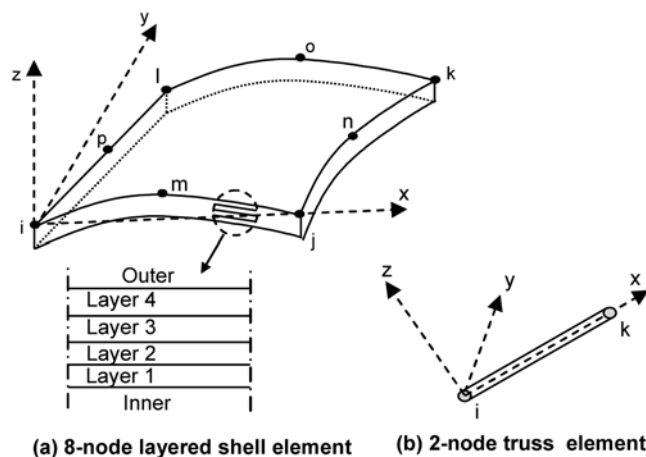


Fig. 5 Elements used in the numerical analysis

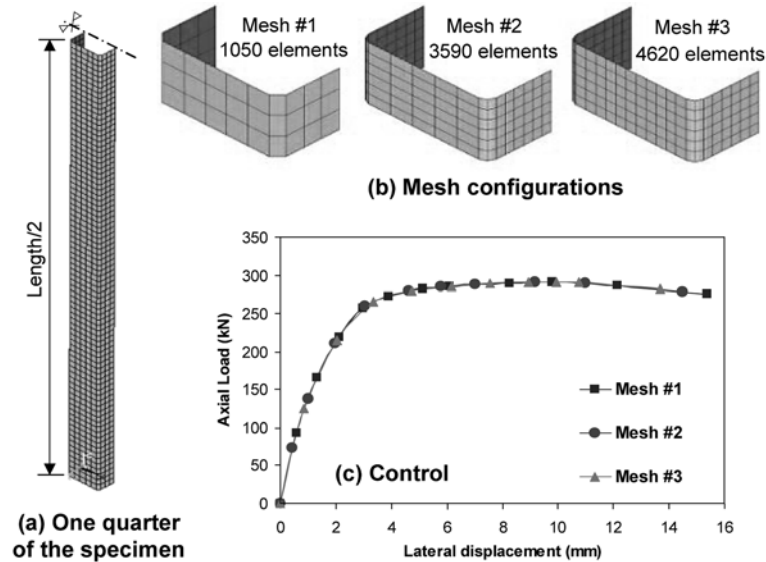


Fig. 6 Mesh refinement and results

model beyond mesh #1. However, the computer run-time dramatically increases with refining the mesh size. As such, mesh #1 was used in all the analyses that followed.

### 3.2 Loading and boundary conditions

The FEM model simulated only one quarter of the specimen by introducing two planes of symmetry, one vertical plane in the longitudinal direction along the full length and another horizontal plane in the transverse direction at column's mid-length. The hinged ends of the actual columns, which are shown in Fig. 4(c), were modeled using a thick plate at the column's end. This plate was restrained from translation in the transverse plane but the translational degrees of freedom of this plate in the longitudinal direction of the column were released to allow for applying axial loads and also all rotational degrees of freedom were released to allow for rotation.

### 3.3 Geometric imperfections

As was concluded in the experimental study, the variation of geometric imperfections among different specimens led to inconsistency of results, which resulted in some difficulties in assessing the effect of FRP strengthening technique. Therefore, the real imperfection values, based on the experiments, were introduced in the FEM at mid-length to initiate the buckling mode (overall buckling) suggested based on the buckling analysis (first stage analysis) and used throughout the verification process. The imperfection values were 6.6, 0.92, 7.04, 2.04, and 5 mm for control, 1L-2S, 3L-2S, 5L-2S, and 3L-4S specimens, respectively (Shaht and Fam 2006).

### 3.4 Material properties

As mentioned earlier, the first stage of the numerical simulation was essentially a linear elastic analysis

of the control column, in which the stiffness of the structure remained unchanged. As such, only the values of Young's modulus and Poisson's ratio of steel were defined (200 GPa and 0.30, respectively). However, the second stage of the numerical simulation comprised a non-linear analysis, in which the stiffness of the structure changes as it deforms. The steel non-linearity (plasticity) was accounted for in the FEM by specifying a bi-linear isotropic hardening model, as shown in Fig. 1(c). The tangent modulus for the steel was assumed equal to 0.5 percent of its elastic modulus (Bruneau *et al.* 1998). For FRP, unidirectional elastic properties were assigned, namely Young's moduli of 20 GPa and 230 GPa for glass- and carbon-FRP, respectively. The compressive strain value of the CFRP was limited to 0.13% as discussed earlier.

### 3.5 Residual stresses

Residual stresses affect the behaviour of steel structures and are normally induced during the manufacturing process. They typically result in a reduction of the flexural rigidity of slender columns, and consequently a lower buckling load may result (Weng 1984). Although residual stresses are self-equilibrating, the cross sectional effective moment of inertia changes when parts of the section reach their yielding strength. Yielding is initiated first in those portions of the cross section having large compressive residual stresses. An extensive experimental investigation of the residual stresses of hollow structural cold-formed steel shapes was performed by Davison and Birkemoe (1983) and Weng and Pekoz (1990). The magnitudes of the measured residual stresses were found to vary, approximately from 25 to 70 percent of the material yield strength, depending on the manufacturing process.

Stub-column tests are typically used in lieu of coupon tests to provide the average compressive stress-strain curves, including the residual stresses effect (Bjorhovde and Birkemoe 1979). This type of tests demonstrates the overall column performance at very low slenderness ratio, in the absence of overall instability. The capacity of these columns is achieved when all fibres reach the yield stress and the corresponding load is defined as the yield load. Because of residual stresses, short columns do not show a distinct yield point, but rather a gradual transition from the linear elastic behaviour to the fully plastic plateau, as a result of gradual yielding. The magnitude of residual stresses  $\sigma_{rs}$  can then be estimated by evaluating the difference between the proportional limit stress and the maximum stress levels. Experimental short column tests have been conducted by the authors on 175 mm long HSS columns of the

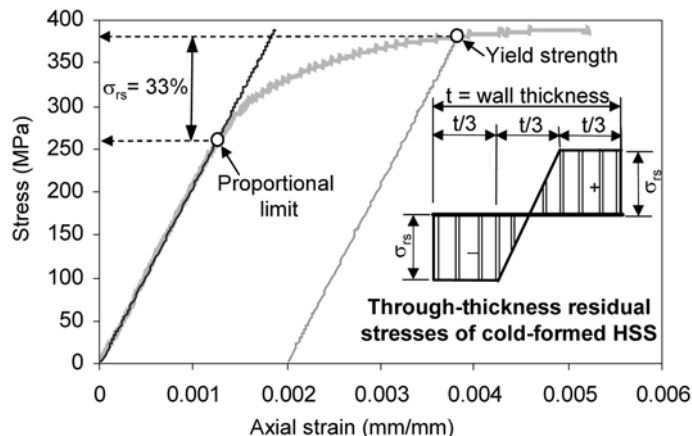


Fig. 7 Evaluation of magnitude of residual stress using stub compression test

same HSS sections used for the slender columns (Shaat and Fam 2006) and the average stress-strain curve is shown in Fig. 7. The behaviour shows a proportional limit stress of 255 MPa and a maximum compressive strength of 382 MPa, which is essentially the specified yield strength for this steel ( $\sigma_y$ ). These two levels of stress indicate that the magnitude of residual stress is in the order of 33 percent of the yield strength. In the proposed FEM, the through-thickness residual stress distribution is idealized as shown in the schematic drawing in Fig. 7, as suggested by Davison and Birkemoe (1983) and by Chan *et al.* (1991), where  $\sigma_{rs}$  equals to  $0.33 \sigma_y$ .

#### 4. Verification of finite element model

The finite element model predictions are verified using the experimental results by Shaat and Fam (2006) as well as another analytical approach (Shaat and Fam 2007), as shown in Figs. 2 and 3 for the five tested specimens, in terms of both the axial load versus axial and lateral displacements, respectively.

The analytical approach (Shaat and Fam 2007) is based on the following Eqs. (1) and (2) (Allen and Bulson 1980), which represent closed form solutions for the axial and lateral displacements of a long column. The equations, however, are only valid within the elastic range.

$$\delta_{axial} = \frac{PL}{E_s A_t} \quad (1)$$

$$\delta_{lateral} = e' \left( \frac{\sin(\pi x / L)}{1 - (P / P_{cr})} - 1 \right) \quad (2)$$

where  $e'$  is the initial imperfection of the column in the form of lateral off-set at its mid-height,  $x$  is the distance at which lateral displacement is calculated,  $L$  is the length of the column,  $P$  is the applied load,  $E_s$  is Young's modulus of steel and  $P_{cr}$  is the Euler buckling load, given by:

$$P_{cr} = \frac{\pi^2 E_s I_t}{L^2} \quad (3)$$

In the previous equations, both the transformed cross-sectional area  $A_t$  and moment of inertia  $I_t$  are introduced by the authors for FRP-retrofitted columns in lieu of the steel section properties and are calculated as follows:

$$A_t = A_s + \sum_{i=1}^n \left[ \frac{E_{f_i}}{E_s} A_{f_i} \right] \quad (4)$$

$$I_t = I_s + \sum_{i=1}^n \left[ \frac{E_{f_i}}{E_s} I_{f_i} \right] \quad (5)$$

where  $A_s$  and  $I_s$  are the cross sectional area and moment of inertia of steel section, respectively.  $A_{f_i}$  and  $I_{f_i}$  are the area and inertia of FRP layer  $i$ , respectively.  $E_{f_i}$  is the effective Young's modulus of layer  $i$  of FRP in the longitudinal direction, and  $n$  is the number of FRP layers. It should be noted that Eq. (2) is valid for lateral displacements of values up to 10% of the length ( $\delta \leq L/10$ ) (Allen and Bulson 1980). Modifications for Eqs. (1) and (2) have been introduced by Shaat and Fam (2007) to account for steel plasticity and

residual stresses built-in the cold formed section.

In general, the FEM shows very good agreement with the experimental results and the analytical model. The relatively significant difference in specimen 5L-2S is likely due to the initial unsymmetrical imperfect shape of the specimen, where the measured lateral displacements at mid-length were not necessarily the maximum values of displacement along the length, unlike the FEM results, which are presented at mid-height of the column.

The failure mode predicted by the FEM, which is an overall buckling, as shown in Fig. 4(d), is quite similar to the buckling failure mode observed in the tests (Fig. 4(a)). The deformed cross section at mid-length of the tested specimen, where inward buckling of the compression flange and outward buckling of the two side webs have occurred is shown in Fig. 4(b). This deformed shape was revealed after the test by cutting the specimen at mid-length. Figs. 4(e, f and g) show the same pattern of deformation predicted by the FEM, in terms of the displacement contours in both x- and z-directions (displacements within the cross sectional plane) as well as the nodal rotation about the specimen's longitudinal axis ( $R_y$ ). The resemblance of Figs. 4(e, f and g) to Fig. 4(b) clearly demonstrates the reliability of the model.

## 5. Parametric study

The FEM has been used in a parametric study to examine the effects of several parameters on the behavior of HSS steel columns strengthened with CFRP sheets. A total of 30 HSS columns with the same cross sectional dimensions and material properties as those used in the experiments were analyzed, where FRP was installed on two opposite sides of the column. The parameters considered were the number of CFRP layers (1, 3, 5, and 7), geometric imperfection (Length/500, Length/1000, and Length/2000), slenderness ratios ( $kL/r = 68, 90, \text{ and } 160$ ) and percentage of residual stresses (25%  $\sigma_y$ , and 50%  $\sigma_y$ ).

The following identification system was adopted to distinguish the various cases. The first number represents the slenderness ratio ( $kL/r$ ), while the second number describes the geometric imperfection. These two numbers are followed by a 'number-letter' combination such as "3L" to identify the number of CFRP layers. Another number describing the percentage of residual stress is added at the end. For control columns, the 'number-letter' combination will be replaced by the word "control". For example, "68-500-5L-25" describes a strengthened column that has a slenderness ratio of 68, a geometric imperfection of (Length/500), and strengthened with five layers of CFRP (applied on two opposite sides of the column) and has a residual stress value of 25 percent of its yield stress.

### 5.1 Results of parametric study

A summary of the FEM results, including the maximum loads, lateral displacements at maximum loads and axial stiffness, is presented in Table 2. Also given in Table 2 are the percentage increases in axial load and stiffness as well as the percentage reduction in lateral displacement at maximum load for the CFRP-strengthened columns, compared to the control columns.

The predicted load-axial displacement behavior for each group of the strengthened columns, compared to their corresponding control steel columns is shown in Fig. 8. The load-lateral displacement responses for the same groups of specimens are shown in Fig. 9. Fig. 10 shows the effect of each parameter on the percentage increases of strength and axial stiffness as well as the percentage reduction in lateral displacement at maximum load. To facilitate the comparisons, a reinforcement index  $\omega$  is introduced to quantify the amount of FRP reinforcement on the basis of a relative axial stiffness, as given by Eq. (6).

Table 2 Summary of finite element results

Specimen I.D.	$\omega$	Max. load (kN)	% age gain	Axial stiffness (kN/mm)	% age gain	Lateral displacement @ max. load (mm)	% age reduction
68-500-control-25	0	289	---	89	---	11.0	---
68-500-1L-25	0.10	307	6	96	8	10.5	5
68-500-3L-25	0.29	346	20	111	25	10.4	5
68-500-5L-25	0.49	383	33	125	40	9.7	12
68-500-7L-25	0.68	421	46	139	56	9.7	12
68-1000-control-25	0	314	---	89	---	8.8	---
68-1000-1L-25	0.10	333	6	97	9	9.1	-3
68-1000-3L-25	0.29	372	18	111	25	8.5	3
68-1000-5L-25	0.49	411	31	126	42	8.2	7
68-1000-7L-25	0.68	450	43	140	57	7.9	10
68-2000-control-25	0	338	---	89	---	6.7	---
68-2000-1L-25	0.10	355	5	97	9	7.2	-7
68-2000-3L-25	0.29	393	16	112	26	6.7	0
68-2000-5L-25	0.49	432	28	126	42	6.9	-3
68-2000-7L-25	0.68	472	40	140	57	6.5	3
68-500-control-50	0	264	---	89	---	15.7	---
68-500-1L-50	0.10	282	7	96	8	15.6	0
68-500-3L-50	0.29	319	21	111	25	15.3	3
68-500-5L-50	0.49	356	35	125	40	14.6	7
68-500-7L-50	0.68	393	49	139	56	13.8	12
90-500-control-25	0	191	---	67	---	25.9	---
90-500-1L-25	0.10	210	10	72	7	24.7	5
90-500-3L-25	0.29	246	29	83	24	18.1	30
90-500-5L-25	0.49	283	48	94	40	16.5	36
90-500-7L-25	0.68	320	68	104	55	14.6	44
160-500-control-25	0	74	---	36	---	108.8	---
160-500-1L-25	0.10	83	12	39	8	92.6	15
160-500-3L-25	0.29	102	38	46	28	79.8	27
160-500-5L-25	0.49	121	64	52	44	76.3	30
160-500-7L-25	0.68	140	89	58	61	69.4	36

$$\omega = \frac{\sum_{i=1}^n [E_{f_i} A_{f_i}]}{E_s A_s} \quad (6)$$

### 5.1.1 Effect of number of CFRP layers

Table 2 and Figs. 8 and 9 clearly show that increasing the number of CFRP layers result in increasing the axial strength and stiffness of the columns as well as reducing the lateral displacements. This effect is also demonstrated in all graphs of Fig. 10, where the number of layers is reflected by the reinforcement

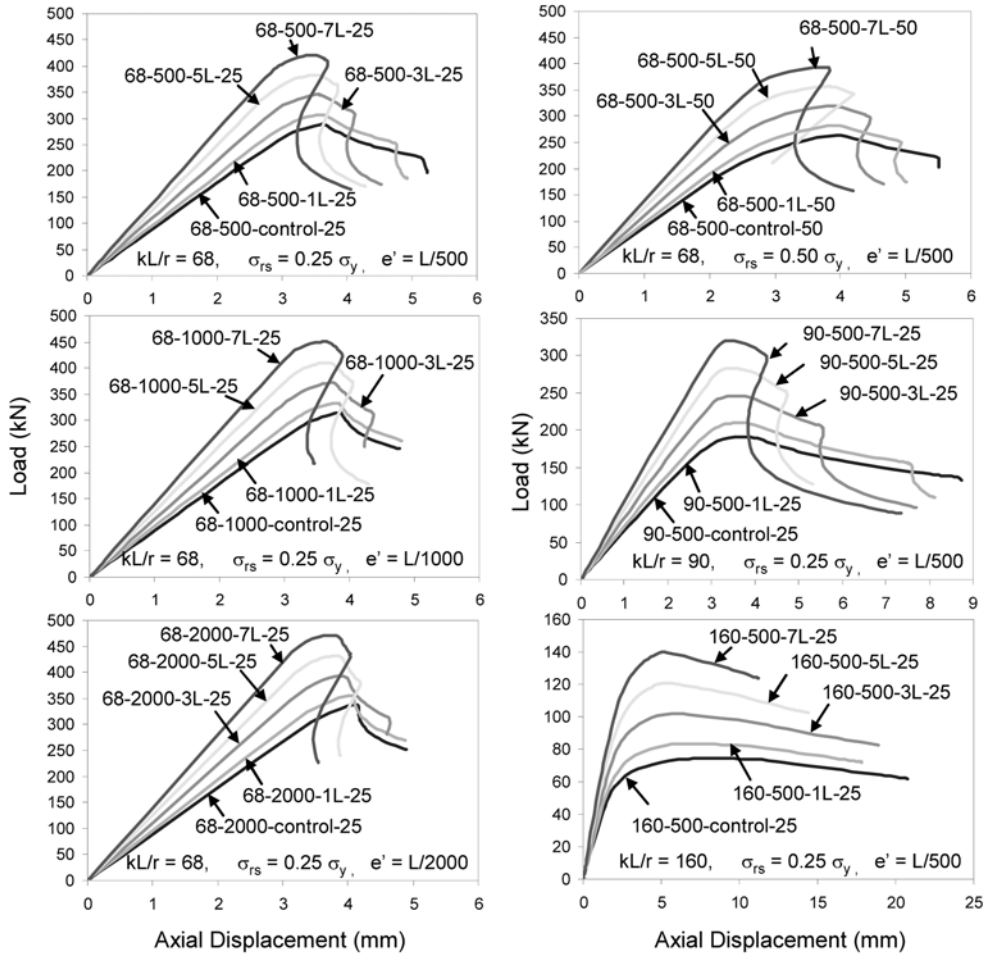


Fig. 8 Load-axial displacement behavior of columns in parametric study

index ( $\omega$ ). Fig. 10 shows that the rate of increase in axial strength is linear for all cases. As the number of layers increase from one to seven layers, the column's strength increased from 6 to 46 percent for columns with  $kL/r = 68$ , from 10 to 68 percent for columns with  $kL/r = 90$  and from 12 to 89 percent for columns with  $kL/r = 160$ .

### 5.1.2 Effect of initial imperfection ( $e'$ )

The initial imperfection of columns greatly affects their axial load capacity. For example, Table 2 shows strengths of 289 kN for specimen 68-500-control-25, and 338 kN for specimen 68-2000-control-25, with imperfections of  $L/500$  and  $L/2000$ , respectively. Although both columns have the same length and cross section, they had 17 percent difference in strength. This emphasizes the crucial rule of the initial imperfection in comparisons between columns.

While the initial imperfection largely affects the columns' maximum load capacity, it has little effect on the percentage increase in strength due to FRP. This percentage was found to be quite similar for the studied levels of imperfection, when each strengthened specimen is compared to its counterpart control

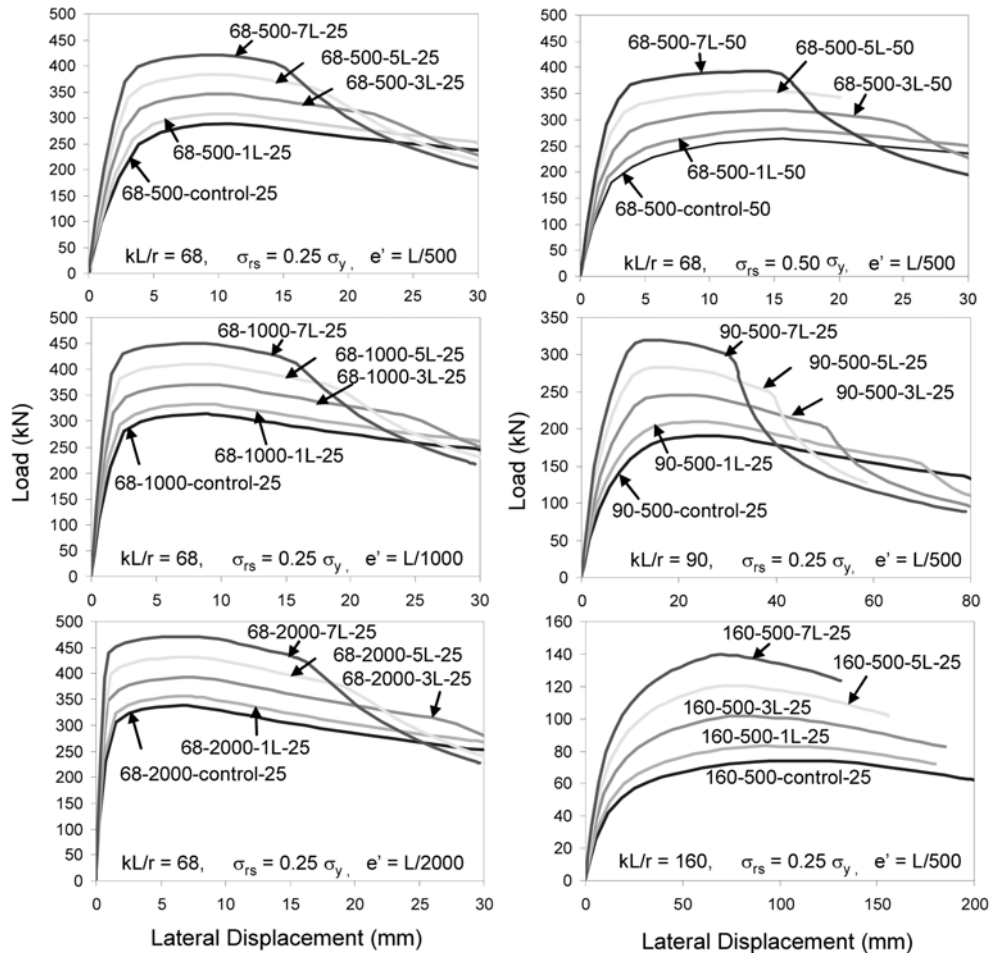


Fig. 9 Load-lateral displacement behavior of columns in parametric study

specimen, as shown in Fig. 10(a). The percentage increases in strength ranged from 5 to 6 percent for specimens strengthened with one layer and from 40 to 46 percent for specimens strengthened with seven layers. The initial imperfection has no effect on the axial stiffness increases, as shown in Fig. 10(b) and a small effect on reduction of lateral displacement, as shown in Fig. 10(c).

### 5.1.3 Effect of column's slenderness ratio ( $kL/r$ )

The effect of columns' slenderness ratio was studied by varying the specimens' length ( $L = 2380$  mm,  $3150$  mm, and  $5600$  mm) to provide slenderness ratios ( $kL/r$ ) equal to 68, 90, and 160, respectively. Figure 10(d) shows that slenderness ratio has a pronounced effect on the effectiveness of FRP-strengthening system. For the same FRP reinforcement index, the strength gain increases substantially as the slenderness ratio is increased. Also, the rate of increase for higher slenderness ratios ( $kL/r = 160$ ) is higher than those of lower slenderness ratios ( $kL/r = 68$  and  $90$ ). The percentage increases in axial stiffness due to increasing the reinforcement index is marginally affected by the different slenderness ratios, as shown in Fig. 10(e). It can also be noted that the percentage reduction in lateral displacement at maximum load increases with

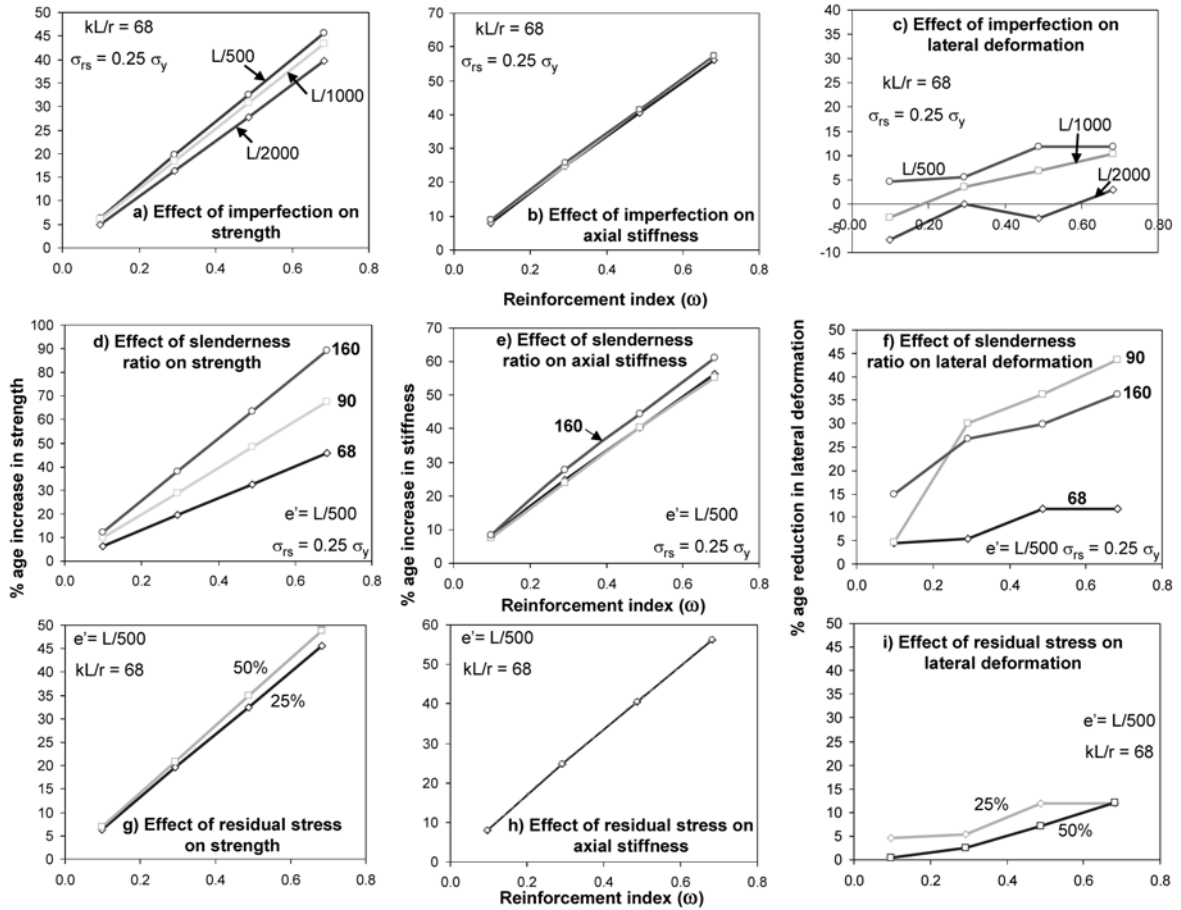


Fig. 10 Summary of results of parametric study

increasing slenderness ratio at small reinforcement indices but tends to reduce after a certain slenderness ratio, for higher reinforcement indices, as shown in Fig. 10(f).

#### 5.1.4 Effect of residual stresses

The level of built-in residual stresses has a marginal effect on both percentage increase of strength and percentage reduction of lateral deformation, as shown in Fig. 10(g and i) and no effect on percentage increase of axial stiffness, as shown in Fig. 10(h) as it mainly affects the initiation of yielding of the column.

## 6. Conclusions

In this paper, a numerical investigation has been presented on the behavior of axially loaded slender HSS steel columns strengthened with longitudinal CFRP sheets. A finite element model (FEM) accounting for geometric and material non-linearities has been developed and successfully verified against both experimental and other analytical studies. A parametric study has been performed to study the effects of

number of CFRP layers, magnitude of residual stress, value of initial imperfection of the steel columns, and columns' slenderness ratio. The following conclusions are drawn:

1. Strengthening of slender HSS steel columns using adhesively bonded high modulus CFRP sheets is a quite effective technique for increasing the axial strength and stiffness as well as delaying overall buckling of the column by reducing lateral displacements.
2. The axial strength of slender HSS columns is quite sensitive to the initial inherent imperfection (out-of-straightness), however, the percentage gain in axial strength due to CFRP strengthening is almost independent of the level of imperfection. The percentage reduction in lateral displacement, on the other hand, is higher for columns with higher initial imperfections.
3. The higher the slenderness ratio of the column, the higher the gain in axial strength due to CFRP strengthening, for the same amount of CFRP.
4. The level of residual stresses has minor effects on the effectiveness of strengthening slender columns with bonded CFRP material.

## Acknowledgement

The authors wish to acknowledge the financial support provided by the Natural Sciences and Engineering Research Council of Canada (NSERC).

## References

- Abushaggar, M. and El Damatty, A. A. (2003), "Testing of steel sections retrofitted using FRP sheets", *Annual Conference of the Canadian Society for Civil Engineering*, Moncton, Nouveau-Brunswick, Canada. June, 4-7, (CD-ROM).
- Allen, H. G. and Bulson, P. S. (1980), *Background to Buckling*, McGraw-Hill Book Company (UK) Limited. S.
- ANSYS Inc. ANSYS User's Manual, Revision 7.1.
- Bjorhovde, R. and Birkemoe, P. C. (1979), "Limit states design of HSS columns", *Canadian J. Civ. Eng.*, **6**, 275-291.
- Bruneau, M., Uang, C. and Whittaker, A. (1998), *Ductile Design of Steel Structures*, McGraw-Hill, New York.
- Canadian Standards Association, CAN/CSA-S16.1-01, Limit States Design of Steel structures, Mississauga, Ontario.
- Chan, S. L., Kitipornchai, S. and Al-Bermani, F. G. A. (1991), "Elasto-plastic analysis of box-columns including local buckling effects", *J. Struct. Eng.*, ASCE, **117**(7), 1946-1962.
- Davison, T. A. and Birkemoe, P. C. (1983), "Column behaviour of cold-formed hollow structural steel shapes", *Canadian J. Civ. Eng.*, **10**, 125-141.
- Jun Deng, Lee, M. M. K. and Moy, S. S. J. (2004), "Stress analysis of steel beams reinforced with a bonded CFRP plate", *Composite Struct.*, **65**, 205-215.
- Kulak, G. L. and Grondin, G. Y. (2002), "Limit states design in structural steel", Canadian Institute of Steel Construction, Alliston, Ontario, Canada.
- Sen, R., Liby, L. and Mullins, G. (2001), "Strengthening steel bridge sections using CFRP laminates", *Composites Part B: Engineering*, **32**, 309-322.
- Shaat, A., Schnerch, D., Fam, A. and Rizkalla, S. (2004), "Retrofit of steel structures using fiber-reinforced polymers (FRP): State-of-the-art", Transportation Research Board (TRB) Annual Meeting, Washington, D.C., USA, CD-ROM (04-4063).
- Shaat, A. and Fam, A. (2006), "Axial loading tests on short and long hollow structural steel columns retrofitted using carbon fibre reinforced polymers", *Canadian J. Civ. Eng.*, **33**, 458-470.

- Shaat, A. and Fam, A. (2007), "Fiber-element model for slender HSS columns retrofitted with bonded high modulus composites", *J. Struct. Eng.*, ASCE, **133**(1), 85-95.
- Weng, C. C. (1984), "Cold-bending of thick steel plates at low R/t ratios", Master's thesis. Cornell University, at Ithaca, N.Y.
- Weng, C. C. and Pekoz, T. (1990), "Residual stresses in cold-formed steel members", *J. Struct. Eng.*, ASCE, **116**(6), 1611-1625.

## Notation

$A_{fi}$	: area of FRP layer number $i$
$A_s$	: cross sectional area of steel
$A_t$	: transformed cross sectional area
$e'$	: imperfection
$E_{fi}$	: Young's modulus of FRP layer number $i$ in the longitudinal direction
$E_s$	: Young's modulus of steel
$i$	: layer number
$I_{fi}$	: moment of inertia of FRP layer number $i$
$I_s$	: moment of inertia of steel
$I_t$	: transformed moment of inertia
$L$	: length of column
$n$	: number of FRP layers
$P$	: applied load
$P_{cr}$	: euler buckling load
$t$	: thickness of HSS
$x$	: distance along the column axis from one end
$\delta_{axial}$	: axial deflection
$\delta_{lateral}$	: lateral deflection
$\sigma'_{rs}$	: residual stress
$\sigma'_y$	: yield strength of steel
$\omega$	: reinforcement index

CC